ECS Transactions, 78 (1) 521-532 (2017)
10.1149/07801.0521ecst ©The Electrochemical Society

Physico-Chemical Characterisation of $Ce_{0.7}Sr_{0.3}Fe_{0.9}Ir_{0.04}Co_{0.06}O_{3-\delta}$ (CSFIC) Cathode Material for Application in Low Temperature SOFCs

C. B. Njoku[a,b], B. O. Omondi[a], P. G. Ndungu[a,c]

[a] School of Chemistry and Physics, Westville Campus, University of KwaZulu-Natal
Private Bag X 54001, Durban 4000, South Africa
[b] Department of Chemistry, Durban University of technology, Steve Biko Campus
P.O Box 1334, Durban 4000, South Africa
[c] Department of Applied Chemistry, Doornfontein Campus, University of Johannesburg
P.O. Box 17011, Doornfontein 2028, Johannesburg, South Africa

In this study, sol-gel technique was used to synthesize the cathode $Ce_{0.7}Sr_{0.3}Fe_{0.9}Ir_{0.04}Co_{0.06}O_{3-\delta}$ (CSFIC) perovskite material and it was then tested for its characteristic application in solid oxide fuel cell. The textural properties were tested using Raman spectroscopy and Fourier transform infrared spectroscopy. The crystal structure was tested using X-ray diffraction and the morphology and microstructure were examined using scanning electron microscopy and high resolution transmission electron microscopy. The power density and current density were measured with a Nuvant™ potentiostat and galvanostat from Fiaxell SOFC Technologies connected to the cell setup. These properties were tested for their potential application in low temperature solid oxide fuel cells from 300 to 500°C. It exhibited a current density of 772.35 mA/cm^2 and a power density of 455.49 mW/cm^2.

Introduction

Power generation has been diversified over the last decade by the discovery of alternative sources of power such as solid oxide fuel cells (SOFCs) (1). Solid oxide fuel cell technology has several interesting features, such as proficient and adept generation processes and low to zero toxic emissions (2). SOFCs have higher energy conversion efficiencies and can be combined with heat generation to produce electricity (3). These have been used to generate power in residential and commercial buildings, large-size stationary power facilities, auxiliary power batteries for transportation vehicles and mobile applications (4,5).

In recent times great efforts have been made to reduce the cell operational temperature to reduce high cost of production and improving balance in the plant component materials; hence, the research drive to develop SOFCs for low-intermediate temperatures between 300-600°C (6). The performance of low-temperature SOFC can be improved by decreasing the electrolyte thickness and by introducing alternative electrode materials that can perform better, with high ionic and electronic conductivity under reducing and oxidative conditions (7-11), and also by introducing materials with high catalytic activity for fuel oxidation and developing methods to minimize energy losses in

the system (12-15). Other benefits for reducing SOFC operational temperature includes the use of metal supported fuel cells which are beneficial because of their minimal cost, excellent thermal conductivity, superior power conversion, improved feasibility, and quicker start-up time (16,17).

In this study, composites of porous nickel oxide and samarium doped ceria were used as cermet anode. The mixture contained a high volume fraction of Ni oxide because it improves the electronic percolation path and expands the electrocatalytic active region in the electrode (18,19). Doped ceria was also used as an electrolyte because it is compatible with the cermet anode; it has been researched to have high conductivity, mixed proton and oxygen ionic conductivity at low temperatures between 300 and 600°C (20,21). Platinum group metals such as iridium were used in this study to produce the cathode material. The use of this material as part of an electrode material is limited, and it has been shown by Huerta et al that the electrochemical properties of iridium oxide on yttrium-stabilized zirconia (YSZ) are suitable for SOFC applications in the temperature range 573–873 K (22). Iridium was used to synthesize $Ce_{0.7}Sm_{0.3}Fe_{0.9}Ir_{0.04}Co_{0.06}O_{3-\delta}$, nanocomposite as a cathode material for low temperature SOFC. The perovskite nanocomposite was prepared by the novel sol-gel method; this technique is a relatively simple method that can be easily modified to synthesize complex metal oxide formulations. The perovskite was further calcined at 800–1000°C and the electrochemical performance was investigated using humidified hydrogen and air as gases for the system.

Experimental Methods

Synthesis of Nanocrystalline Materials

Cerium (III) acetylacetonate hydrate, (99.9 % purity), iron(III) acetylacetonate (97% purity), samarium (III) acetylacetonate hydrate (99.9%), cobalt (II) acetylacetonate hydrate (99 % purity), and Pluronic F-127 were purchased from Sigma-Aldrich (Pty) Ltd, South Africa. Iridium (III) acetyl acetonate hydrate was purchased from Alfa Aesar UK. These chemicals were used without further purification.

In this synthesis, 1.2102 g of cerium (III) acetylacetonate hydrate, 1.1820 g of iron (III) acetylacetonate hydrate, 0.5640 g of samarium (III) acetylacetonate hydrate, 0.0930 g of cobalt (II) acetylacetonate hydrate and 0.0758 g of iridium (III) acetylacetonate hydrate were weighed and added into a mixture of 15 mL of deionized water and 50 mL of ethanol. 4.00 g of Pluronic F-127 was added to the mixture and then sonicated for 30 mins in an ultrasound bath (UMC 20, 50 kHz). The solution formed was then placed on a hot plate and heated to 80°C and stirred at 180 rpm for 30 mins. The samples were then dried for 24 hours in an oven at 200°C and then calcined in a muffle furnace (Kittec Squadro 1350) at a heating rate of 2°C/min for 12 hours, to final temperatures of 800°C, 900°C, and 1000°C.

Synthesis of Electrolyte

To synthesize the electrolyte, 0.200 g of samarium (III) acetylacetonate and 0.534 g of cerium (III) acetylacetonate were mixed with a solution of ethanol (50 mL) and

deionized water (15 mL) in an ultrasound bath. After 30 mins, the solution was heated on a hotplate, while stirring, for 20 mins (120 rpm at 80°C). Samples were then calcined at 850°C for 5 hours at 2°C/min in a muffle furnace. The samarium doped ceria (SDC) material formed was hand mixed with sodium carbonate (Na_2CO_3) in a mass ratio of 60:40% to form SDC/Na_2CO_3 electrolyte.

Characterization

The structural properties of the perovskite nanocomposite were characterized using high resolution transmission electron microscopy (HR-TEM), powder X-ray diffraction (XRD) and infrared spectroscopy. The morphology was characterized using scanning electron microscopy (SEM). The XRD patterns were obtained using Siemens D8 Advance diffractometer with a CuKα radiation source operating at 40 kV and a wavelength of 1.5412 Å. The XRD diffractogram was recorded from $20° \leq 2\theta \leq 90°$ at a scan speed of 2°/min. The mean crystallite size 'D' was calculated using Scherer equation (23):

$$D = 0.9\lambda/\beta cos\emptyset \quad [1]$$

where: ƛ is the X-ray wavelength (1.5405 Å), β is the full width at half maximum of the diffraction line and $\emptyset$ is the diffraction angle.

During the HR-TEM analysis, small amounts of the sample were dispersed in ethanol and then shook in an ultrasound bath, then drop-dried onto a carbon coated copper TEM grid, and examined on a JOEL 2100 HRTEM (200 kV accelerating voltage, beam current of 110 μA and a current density of 2.4 pA/cm^2). For the SEM observations, powders were placed onto carbon tape coated aluminum stubs and gold coated on a ZEISS FEGSEM Ultra Plus. Infrared spectra were analyzed on a Perkin Elmer 1200 FTIR.

Single Cell Fabrication

The cathode cells were prepared by forming the materials with a 20-ton press and a 1.3 cm die kit. 0.1535 g of the CSFIC material was placed into the die kit mold and 15 tons of pressure was then applied using a 20-ton press. 0.2100 g of SDC/Na_2CO_3 was used to prepare the electrolyte using the same method. 0.4500 g of NiO-SDC was used to make the anode using the same method. The electrolyte was sandwiched between the cathode and the anode. The discs had a total active area of 1.327 cm^2. The cathode, electrolyte and anode discs were then heat-treated at 1050°C for 2 hours at a heating rate of 5°C/min. The electrolyte was estimated to be 0.02 cm thick, the cathode was 0.015 cm thick and the anode was 0.03 cm thick.

Electrochemical Performance Test

To analyze the electrochemical properties, the electrolyte disc was sandwiched between the anode and cathode discs and then placed in the open flange test set-up from Fiaxell SOFC Technologies™. This set-up was designed for the cell sizes, and platinum meshes were used as contact components, to act as combined current collector and gas

distributor. The test-bed was placed in a Kittec Squadro muffle furnace and linked to appropriate gas tight fittings for the delivery of humidified air and hydrogen (~ 4-20% water) gas to the cell. The wire of the mesh was connected to a Nuvant™ Powerstat 05 potentiostat and galvanostat where the current and voltage from the cells were measured. The polarization curves were recorded between 300°C - 500°C.

Results and Discussion

Powder XRD Analysis

Figure 1 shows the XRD diffractogram of CSFIC cathode material calcined at 800°C, 900°C, and 1000°C. These exhibited 3 phases, namely cerium oxide (cerianite) structure, iron samarium oxide ($FeSmO_2$) structure and iron oxide (Fe_2O_3) hematite structure with peaks observed at 2θ values of 28.54°, 33.09°, 47.49°, 56.36°, 59.24°, 63.14, 69.49°, 76.65°, 79.26°, 88.54°, 95.63° indexed to 111, 200, 220, 311, 222, 301, 331, 420, 422, and 532, respectively. The average lattice parameter a is 5.41 Å for the predominant CeO_2 phase and the Bravais lattice is a face centered cubic unit cell. The calculations are shown in Equation 2 to 4. This was calculated with full proof suite software (24).

$$\text{Lattice parameter} = \lambda/2 \times sin\emptyset \times \sqrt{h^2 + k^2 + l^2} \quad [2]$$

where: λ = wavelength of the instrument, θ = 2 theta value/2. The mass of the unit cell for all samples was 1.3443 x 10^{-22} g, and this was calculated using the following equation:

$$\text{Mass of Unit Cell (M)} = \frac{(4atoms)(MolarMass)}{6.02\times10^{23}\,atoms/mol}\left[\frac{10^{-6}Mg}{g}\right] \quad [3]$$

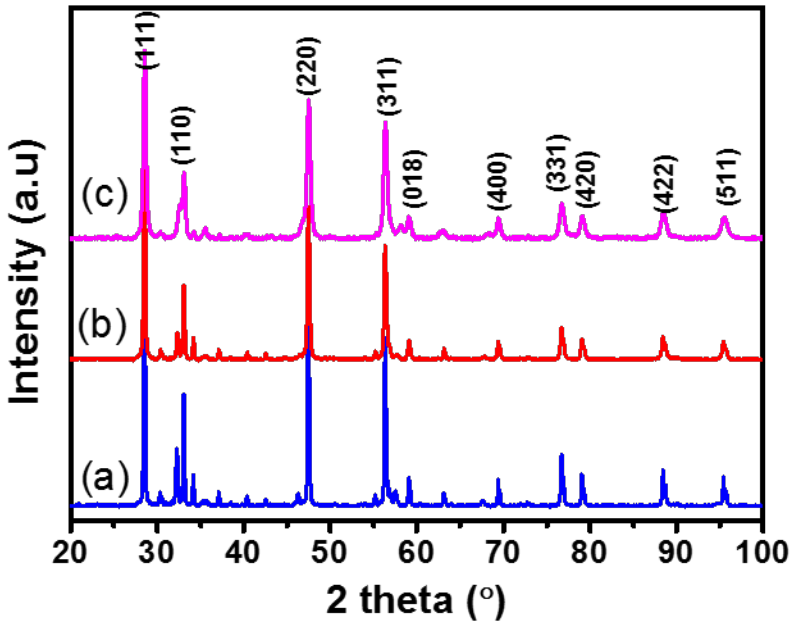

Figure 1. The XRD diffractogram of CSIFC cathode calcined at (a) 1000°C, (b) 900°C and (c) 800°C.

The volume density of the unit cell was 7.41g/cm^3, and the following equation was used to calculate this value:

$$\text{Volume Density} = \frac{mass\,(unit\ cell)}{Volume\,(unit\ cell)} \quad [4]$$

Volume of unit cell was calculated to be 1.5984 x 10^{-23} cm^3 (from $v = a^3$ where a = $4R/\sqrt{2}$)

With increasing calcination temperature, the peaks of the diffractogram become sharper, the peak intensities increased, and then decreased from the lowest 2θ values to the highest 2θ values. 111 peak was the most intense peak which results from an increase in temperature increases the intensity of the XRD peak. Table I shows the full width at half maximum (FMWH), crystallite sizes and the average particle sizes. This revealed that samples calcined at 1000°C exhibited larger crystallite size and the sample calcined at 800°C exhibited the smaller crystallite size. This can be confirmed on the HRTEM micrograph which showed smaller particles at 800°C. Recently it has been written that 111 active peak is the least active surface for the removal of oxygen (25) and the presence of the 111 plane proofs the presence of Ce^{3+} in these materials (26). The presence of Ce^{3+} in fluorite ceria structure produces oxygen vacancies to sustain electrostatic stability as shown in Equation 5 (27):

$$4Ce^{4+} + O^{2-} \rightarrow 4Ce^{4+} + 2e^- / \boxdot + \frac{1}{2}O_2 \rightarrow 2Ce^{4+} + 2Ce^{3+} + \boxdot + \frac{1}{2}O_2 \quad [5]$$

where $\boxdot$ represents an empty position (anion-vacant site) originating from the removal of O^{2-} from the lattice.

Table I. The Crystallite size, and Average particle size of CSIFC cathode calcined at (a) 800°C, (b) 900°C, and (c) 1000°C.

Calcination Temperature (°C)	Crystallite Size (nm)	Average Particle Size (nm)
800	19.80 ± 0.63	20.04
900	37.50 ± 1.25	39.05
1000	46.85 ± 2.24	49.88

FTIR Analysis

Figure 2 shows representative absorbance peaks at 1489.03 cm^{-1} for the 1000°C calcined sample and 1472.02 cm^{-1} for 900°C calcined sample, which are attributed to C = O bonds from carbonate impurities for samarium doped ceria oxide (28). Vibrational bands at 1035.11 cm^{-1} were visible for the samples calcined at 1000°C, 1036.11 cm^{-1} were visible for the 900°C, 1095.02 cm^{-1} and 1014.08 cm^{-1} were visible for 800°C. These bands are assigned to the metal (M) to oxygen bond vibration, caused by the M-O-M stretching vibration. The variations in the peaks mentioned above are also as a result of the difference in distances between metal to oxygen bond (M-O-M).

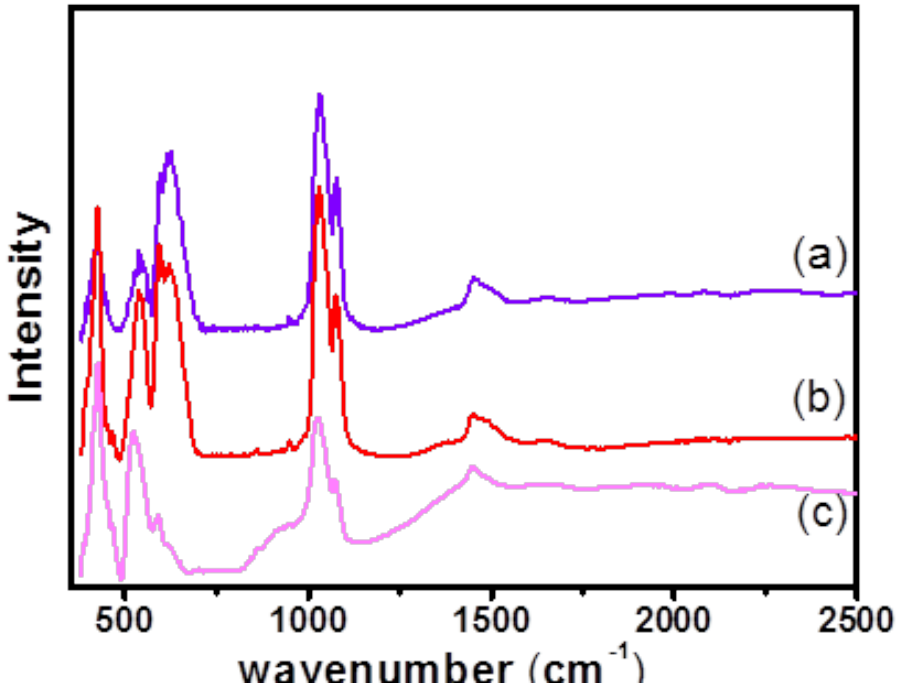

Figure 1. The FTIR spectra of CSFIC cathode calcined at (a) 1000°C, (b) 900°C and (c) 800°C.

Peaks were also evident at the lower region of the spectrum (424.05 cm^{-1}, 425.11 cm^{-1}, 428.10 cm^{-1}) for the samples calcined at 1000°C, 900°C and 800°C, respectively, indicating the formation of spinel metals of common characteristic spinel structures. This is produced by metal~oxygen vibrations in the tetrahedral sites and the peaks observed at 582.04 cm^{-1}, 547.07 cm^{-1} and 535.07 cm^{-1} for 1000°C, 900°C and 800°C respectively are vibrations in the octahedral sites (29,30). According to Waldron (28), the vibration of a unit cell of cubic spinels can be constructed in the tetrahedral (A) sites and octahedral (B) sites. The change in band positions for the different samples is expected because of difference in the M^{+}– O_2– distances for the tetrahedral and octahedral sites. The deduction is also confirmed by XRD analysis (30).

SEM Observations

The SEM observations in Figure 3 show morphology of the perovskite material revealing different particles sizes, the sizes of the particles increased with increasing calcination temperature as shown by the XRD diffractogram calculations. It is assumed that the nanoparticles are arranged in agglomerate formation. The use of surfactant in preparing the perovskite increases the agglomeration separation of the particles and controls the pore spaces. The pore spaces were observed to decrease as the calcination temperature decreased. These pore spaces allow the diffusion of gases through the electrodes. The gases move faster with bigger pore sizes which enhance the performance of the cathode material. This corroborates with the HRTEM micrograph which revealed smaller particle sizes as the calcination temperature decreased.

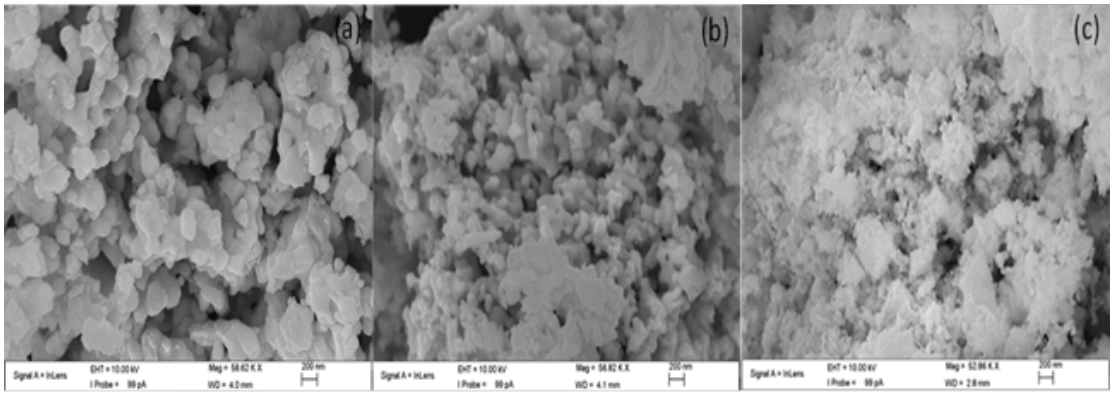

Figure 3. The SEM morphology of CSFIC cathode calcined at (a) 1000°C, (b) 900°C and (c) 800°C.

Figure 4 shows the energy-dispersive X-ray spectroscopy (EDX) analysis of the powders. The EDX analysis identified the individual metal components within the samples and the color maps were done using EDX mapping. From the elemental mapping, a uniform distribution of the metals was shown with no obvious concentration of a particular metal within a specific area. The corresponding weight percentage analysis using SEM-EDX is presented in Table II. This confirmed that the metals were present and the ratios were within reasonable and expected ranges, as seen by the small deviations between the measured weight and the theoretical weight.

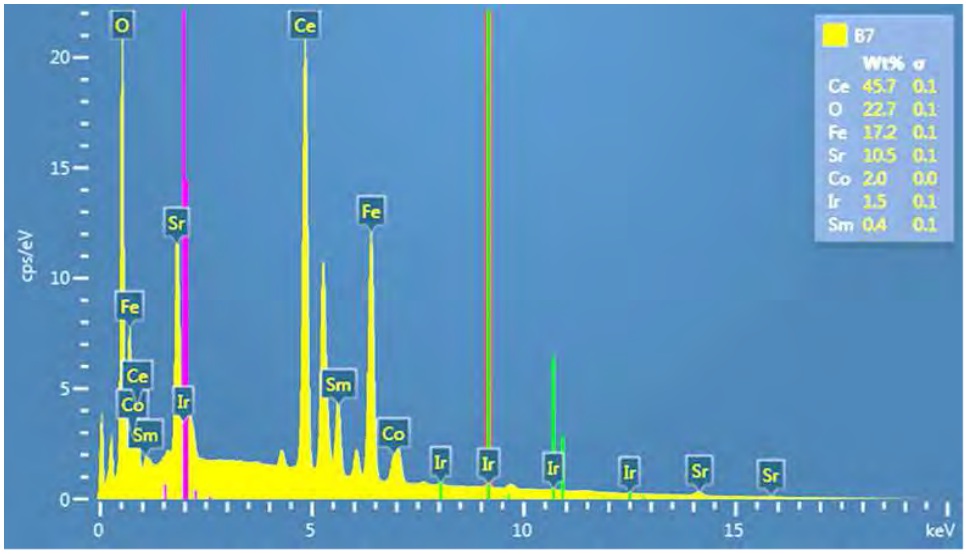

Figure 4. The EDX analysis of the CSFIC cathode calcined at 1000°C.

Table II. The SEM-EDX analysis results from the CSFIC cathode calcined at 1000°C.

Element	Measured (Wt %)	Theoretical (Wt %)
Ce	45.70	43.68
Sr	10.50	11.01
Fe	17.20	20.08
Ir	1.50	1.57
Co	2.00	2.30
O	22.70	20.29

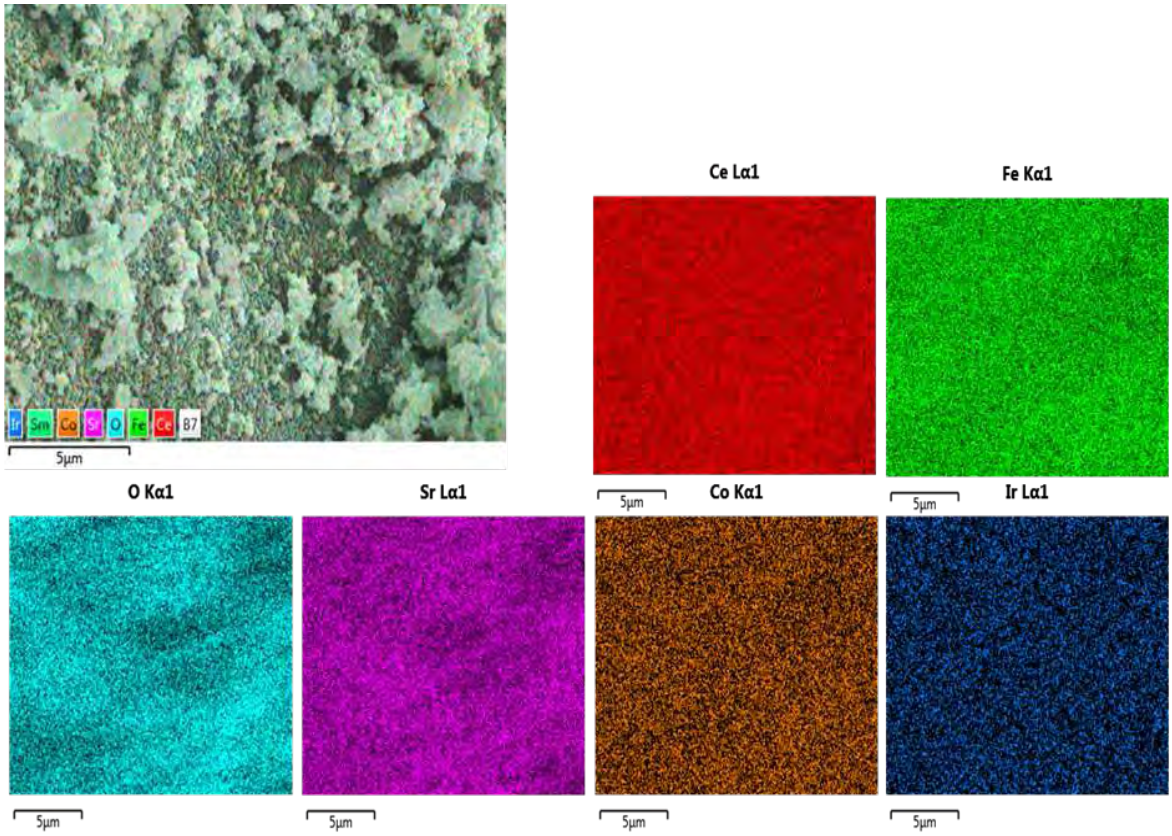

Figure 5. Imaging of the CSFIC cathode calcined at 1000°C by EDX mapping.

HRTEM Observations

The nanoparticles were observed by HRTEM, and representative images are shown in Figure 6. The microstructure showed slight differences, specifically, irregular shapes and the samples calcined at 800°C showed smaller crystalline shapes. The measured lattice distance between the fringes was 0.134 nm indexed to (400), 0.380 nm indexed to (211) and 0.125 nm indexed to (331) for 800°C-1000°C samples, respectively.

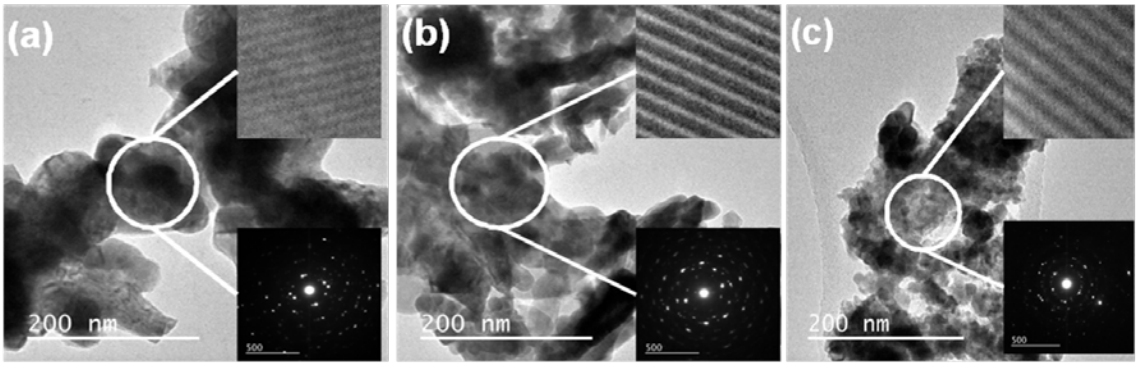

Figure 6. HRTEM micrograph of CSFIC cathode calcined at (a) 1000°C, (b) 900°C and (c) 800°C.

These distances are linked to the XRD as Fe_2O_3 (magnetite) and CeO_2 (fluorite) structures. The presence of CeO_2 fluorite structure in the HRTEM observations, correlate

with the XRD analysis which indicates the samples have some concentration of oxygen vacancies on the surface. The selected area electron diffraction patterns did not show too many significant differences between the samples.

Electrochemical Properties

Polarization Curves. The polarization curves for the CSFIC cathode calcined from 800-1000°C are shown in Figure 7. The results for the analysis were obtained using humidified hydrogen and humidified air (20% water) at temperature intervals of 300-500°C. The OCV values (Figure 8) of the tested cells show a decrease in trend when measured from 300-500°C which was stable at 0.87 V for more than 15 hours for all samples calcined at 500°C. This value does not correspond with the thermodynamic values calculated using Nernst equation. The difference can be attributed to the cell assembly and cell structural composition. The crossover of gases through the electrolyte and this is as a result of using cold powder compacting temperature which could leave residual pores and result in leakage through any connected pores present.

The polarization curves showed a linear fall in voltage as the current densities increased which resulted from the resistance to current flow within the button cell. When current increases, the voltage drop increases as a result of kinetic and ohmic losses within the cell. The power density also increased as the calcination temperatures increased. This can be linked to the structural differences revealed by XRD, HRTEM and Infrared spectroscopy. The presence of a greater amount of oxygen vacancies, and Ce^{3+} within the material framework can allow for improved oxygen reduction kinetics and maybe one of the main reasons for the improved power density at 1000°C.

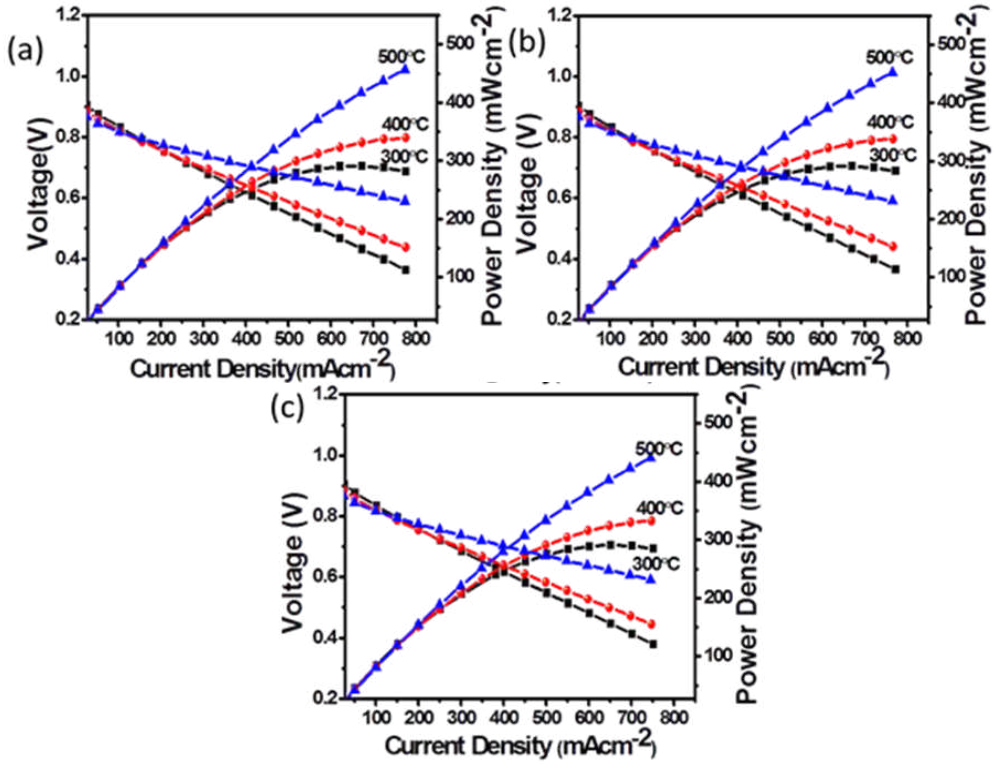

Figure 7. The polarization curve of CSFIC cathode calcined at (a) 1000°C (b) 900°C and (c) 800°C.

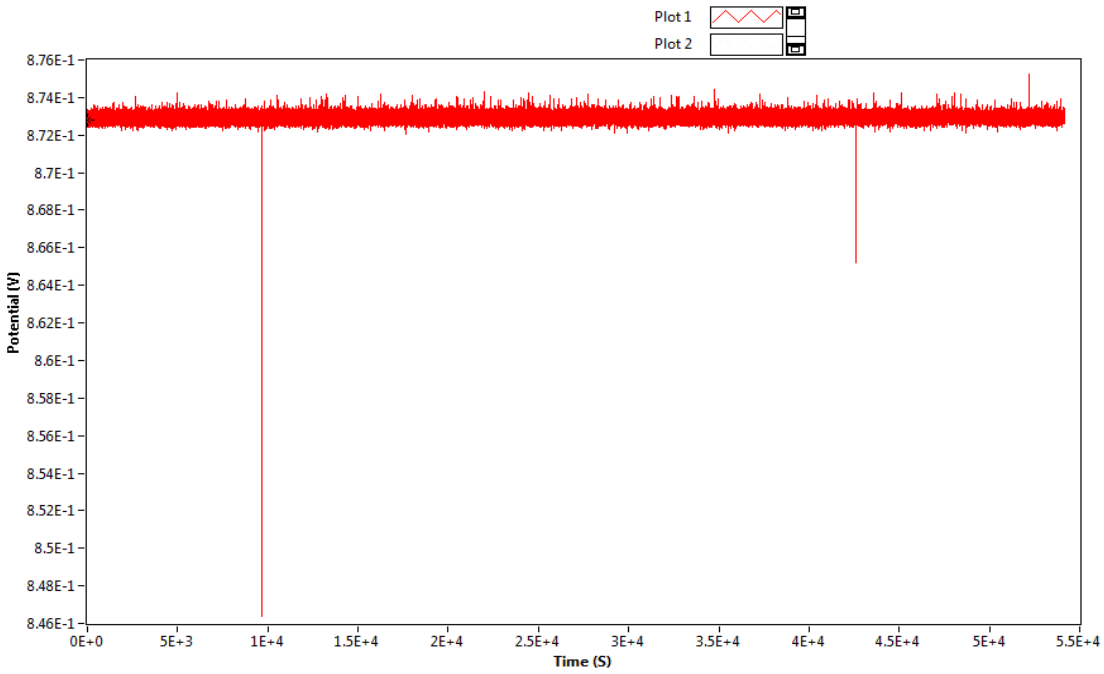

Figure 8. The Open Cell Voltage of CSFIC cathode calcined at 800°C measured at 500°C for 15 hours.

Conclusions

A novel cathode material, CSFIC, was synthesized and characterised using X-ray diffraction, Fourier transform infrared spectroscopy, scanning electron microscopy, high resolution transmission electron microscopy, and tested as an SOFC electrode. FTIR spectra revealed that the cathode material contains spinel metals such as iridium and iron oxides. The increase in temperature caused a shift in bands assigned to metal (M) to oxygen bond vibration, caused by the M-O-M stretching vibration. The variations in the peaks are also as a result of the difference in distances between metal to oxygen bond (M-O-M). XRD analysis confirmed the existence of minor phases of iridium and iron oxides, and corroborates with the FTIR results and supported the notion concerning the presence of Ce^{3+} and oxygen vacancies within the samples. HRTEM analysis revealed the samples had irregular shaped crystallites with differing phase structures as the calcination temperature was increased. SEM observations showed all samples consisted of porous agglomerates. The polarisation curve shows that the sample calcined at 1000°C produced the highest power density of 455.49 mW/cm^2 and a current density of 772.35 mA/cm^2 when measured at 500°C.

Acknowledgements

The authors thank the University of KwaZulu-Natal, for providing access to research facilities used in this research. ESKOM-TESP and NRF of South Africa (Thuthuka programme, Grant No: 76318) for research funds.

References

1. B. G. Pollet, I. Staffell, and J. L. Shang, *Electrochimica Acta*, **84**, 235-249 (2012).
2. J. J. Botti, M. J. Grieve, and C. E. Miller, Delphi Technologies, Inc., *Power generation system and method with exhaust side solid oxide fuel cell*. U.S. Patent 6,655,325 (2003).
3. A. B. Stambouli, and E. Traversa, *Renewable Sustainable Energy Rev., **6***(5), 433-455 (2002).
4. L. Fan, B. Zhu., M. Chen, C. Wang, R. Raza, H. Qin, X. Wang, W. Xioadi, and Y. Ma, *J. Power Sources,* **203**, 65-71 (2012).
5. R. Hui, J.O.Berghaus., C. Decès-Petit, W. Qu, S. Yick, J.G. Legoux, and C. Moreau, *J. Power Sources*, **191**, 371-376 (2009).
6. F. M. L. Figueiredo, and F. M. B. Marques, Electrolytes for solid oxide fuel cells, *Wiley Interdisciplinary Reviews: Energy and Environment*, ***2***(1), 52-72 (2013).
7. J. T. Vaughey, J. R. Mawdsley, and T. R. Krause, *Mater. Res. Bull.,* **42**, 1963, (2007).
8. J. C. Ruiz-Morales, J. C.Vazquez, D. Marrero-lopez, J. T. S. Irvine, and P. Nunez, *Electrochim. Acta,* **52**, 7217 (2007).
9. T. Ikebe, H. Muroyama, T. Matsui, and K. Eguchi, *J. Electrochem. Soc.,* **157**, 970 (2010).
10. X. Huang, H. Zhao, W. Shen, W. Qin, and W. Wu, *J. Phys. Chem. Solids*, **67**, 2609 (2006).
11. X. Li, H. Zhao, F. Gao, Z. Zhu, N. Chen, and W. Shen, *Solid State Ionics*, **179**, 1588 (2008).
12. Z. Shao and S. M. Haile, *Nature*, **431**, 170-173 (2004).
13. A. Atkinson, S. Barnett, R. J. Gorte, J. T. S. Irvine, A. J. McEvoy, M. Mogensen, S. C. Singhal, and J. Vohs, *Nat. Mater.,* **3**, 17-27 (2004).
14. R. M. Ormerod, *Chem. Soc. Rev.,* **32**, 17-28 (2003).
15. K. Sasaki, H. Naohara, Y. Cai, Y. M. Choi, P. Liu, M. B. Vukmirovic, J. X. Wang, and R. R. Adzic, Core-Protected Platinum Monolayer Shell High-Stability Electrocatalysts for Fuel-Cell Cathodes, *Angewandte Chemie International Edition,* **49**(46), 8602-8607 (2010).
16. Z. Wang, J.O. Berghaus., S. Yick, C. Decès-Petit, W. Qu, R. Hui, R. Maric, and D. Ghosh, *J. Power Sources,* **176**, 90-95 (2008).
17. M. C. Tucker, G. Y. Lau., C. P. Jacobson, L. C. DeJonghe, and S. J. Visco, *J. Power Sources*, **175**, 447-451 (2008).
18. B. S. Prakash, S. S. Kumar, and S. T. Aruna, *Renewable Sustainable Energy Rev.,* **36**, 149-179 (2014).
19. J. Di, M. Chen., C. Wang, J. Zheng, L. Fan, and B. Zhu, *J. Power Sources,* **195**, 4695-4699 (2010).
20. A. Tsoga, A. Gupta, A. Naoumidis, and P. Nikolopoulos, *Acta Mater.,* **48**, 4709-4714 (2000).
21. J. Will, A. Mitterdorfer, C. Kleinlogel, D. Perednis, and L. J. Gauckler, *Solid State Ionics,* **131**, 79-96 (2000).

22. A. M Torres-Huerta, J. R. Vargas-García, and M. A. Domínguez-Crespo, *Solid State Ionics,* **178**, 1608-1616 (2007) .
23. C. B. Njoku, P. G. Ndungu, *J. Fuel Cell Sci. Technol.,* **11**, 041010-1 (2014).
24. C. B Njoku, P. G Ndungu, *Mater. Res. Bull.,* **68**, 100-108 (2015).
25. A. Trovarelli, In Catalytic Science Series, Vol. 2; Trovarelli, A., Ed.; Imperial College Press: London, 15 (2002).
26. Z. Wu, M. Li, J. Howe, H. M. Meyer III and S. H. Overbury, *Langmuir,* **26** (21), 16595-16606 (2010).
27. X. Liu, K. Zhou, L. Wang, B. Wang, and Y. Li, *J. Am. Chem. Soc.,* **131**, 3140-3141 (2009).
28. C. Shen, and L. L. Shaw, *J Sol-Gel Sci Technol.,* **53,** 571-577 (2010).
29. Y. B. Bingjun Xu, and M. E. Davis, *Chem. Mater.,* **25**, 1564-1571 (2013).
30. L. Xiangwen, Z. Kebin, W. Lei, W. Baoyi, and L. Yadong, *J. Am. Chem. Soc.,* **131**, 3140-3141 (2009).
31. E. Aneggi, C. deLeitenburg, and A. Trovarelli, *Catal. Today,* **181**, 108-115 (2012).
32. S. Damyanova, B. Pawelec, K. Arishtirova, M. M. Huerta, and J. L.G. Fierro, *Appl. Catal., B.,* **89**, 149-159 (2009).
33. A.V. Korotcov, Y. S. Huang, K. K. Tiong, D. S. Tsai, *J. Raman Spectrosc.,* **38,** 737-749 (2007).